J Therm Anal Calorim (2011) 105:583–590
DOI 10.1007/s10973-010-1232-8

Peculiarities of TiH_2 decomposition

Emília Illeková · Jana Harnúšková · Roman Florek · František Simančík · Igor Maťko · Peter Švec Sr.

ESTAC2010 Conference Special Issue

Abstract The eventual competition between the dehydrogenation and oxidation of TiH_2 powder in the argon, oxygen, and static air atmospheres has been examined in the regime of linear heating using differential thermal analysis (DTA), X-ray diffraction, transmission and scanning electron microscopy coupled to energy dispersive spectroscopy techniques. Three stages of dehydrogenation, R1, R2, and R3, and two different oxidation reactions, O1 and O2, have been identified. The kinetics of individual reactions has been investigated by the Kissinger and Suriñach curve fitting procedures. While the kinetics of O1, O2, and R1 reactions depends on the diffusivities of the external reagent gas, being oxygen, and internal product gas, being hydrogen, the main dehydrogenation stage R2 is controlled by the combined nucleation-and-growth and coalescence kinetics. The effect of pre-annealing of TiH_2 on its subsequent degradation has also been studied. Due to the huge overheating accompanying both oxidation reactions in the DTA set-up, substantial thermal losses have been demonstrated and the method to obtain the true heat of oxidation reactions in metals has been described.

Keywords Titanium hydride · Dehydrogenation · Oxidation · DSC · Kinetics

E. Illeková (✉) · I. Maťko · P. Švec Sr.
Institute of Physics, Slovak Academy of Sciences, Dúbravská cesta 9, 845 11 Bratislava, Slovakia
e-mail: fyziille@savba.sk
URL: http://www.savba.sk/rq

J. Harnúšková · R. Florek · F. Simančík
Institute of Materials and Machine Mechanics, Slovak Academy of Sciences, Bratislava, Slovakia

Introduction

At elevated temperatures titanium hydride (TiH_2) gradually decomposes via a two-stage endothermic reaction evolving H_2 and yielding pure titanium. As the decomposition proceeds between 673 and 1073 K, i.e., at temperatures close to the melting temperatures of aluminum-based alloys, its products find metallurgical exploitation [1]. Namely, due to the progressive evolution of H_2 bubbles in time of the melting and solidification of aluminum (or aluminum-based alloys), the foamy form of Al can be produced. It is sure that the decomposition kinetics directly affects the foaming kinetics, see Fig. 1 [2]. Moreover, in the open air atmosphere, certain relation between the dehydrogenation and the oxidation of titanium should exist [1, 3].

Generally, the decomposition of a metal hydride under non-equilibrium conditions (at linear heating) is a multi-stage process, the mechanism of which is scarcely studied. Generally, differential scanning calorimetry (DSC) is being used for such studies [1, 3–6]. The thermal desorption spectroscopy (TDS) analyses of Fernandez et al. showed linear proportionality between the hydrogen evolved (TDS data) and the heat absorbed (DSC data) in the case of dehydrogenation of TiH_2 [4]. Later, also the reaction model for TiH_2 dehydrogenation was deduced and the rate-controlling process supposed by estimating the activation energy and its variation using the isoconversional method and the thermogravimetry data (TG) by Liu et al. [3].

In this article, the details in the kinetics of the dehydrogenation as well as of the high-temperature oxidation of powdered TiH_2 are studied by the use of the DSC technique. Experimental data are analyzed by the Suriñach curve fitting procedure [7]. The specific roles as well as the mutual relation between the dehydrogenation and the oxidation reactions are investigated.

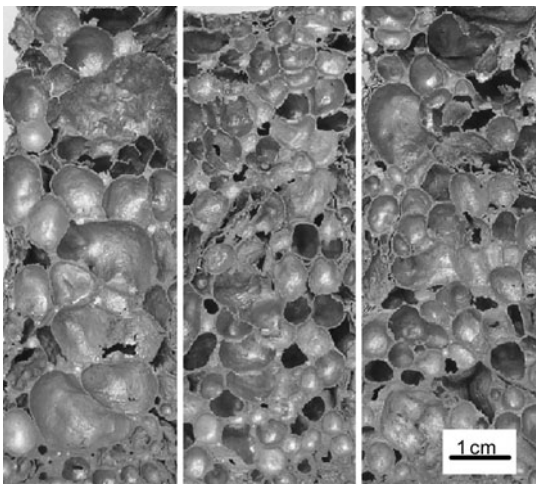

Fig. 1 Al foam with **a** TiH_2 without heat-treatment, **b** TiH_2 heat-treated in air for 15 min at 673 °C, **c** at 718 °C

Materials and methods

Commercial titanium hydride powder, TiH_2, supplied by Chemetall GmbH, Frankfurt (purity 98.8%, nominally <63 μm, average particle size $d = 5$ μm) was examined in the as-produced state and also after various industrial pre-treatments. Pre-treatments were done in industrial-size batches isothermally at 673, 718, or 788 K for 15 min in static air atmosphere. Alternatively, TiH_2 powder produced by Alulight ($d \sim 63$ μm, fraction) was measured.

The thermodynamic stability and the kinetics of observed phase transformations were monitored by high-temperature differential thermal analyzer (DTA) in the mode of DSC using Perkin-Elmer DTA7. Linear-heating regimes using six heating rates, Φ, from 1 to 30 K min^{-1} at temperatures, T, between 300 and 1123 K were used. After the calibration, the error of established quantities is ±2 K and ±4 J g^{-1} for all heating rates. Three types of experiments were realized: (i) the dehydrogenation was followed by measurements in dynamic argon (30 mL min^{-1}), (ii) the oxidation was attained by measuring in dynamic oxygen (30 mL min^{-1}), (iii) the degradation of TiH_2 under non-equilibrium conditions, similar to the industrial ones, was carried out by measuring in static air. Both the input of the reacting gas O_2 and the output of the released gas H_2 were accomplished by locating of always the same big mass of the powdered sample (26 mg) in narrow (3 mm) and deep (7 mm) alumina pans without lids.

The structure of initial, partially heat-treated and product powders was evaluated by X-ray diffraction (XRD) using Cu K_α radiation at room temperature. The structural and chemical analysis of both initial TiH_2 and pre-treated powders were performed by scanning electron microscopy coupled to energy dispersive spectroscopy technique (SEM/EDX) using SDB Quanta 3D 200i. More detailed analysis of pre-treated powders was performed by transmission electron microscopy (TEM) using JEOL 2000 FX.

Results and discussion

Dehydrogenation

Figure 2 shows a typical DSC curve of TiH_2 measured in argon. The dehydrogenation is represented by a massive complex endothermic double peak ($\Delta H \sim 2600$ J g^{-1}) which starts at the temperature $T_x > 700$ K and is finished above 1123 K, the highest temperature of our measurements. Accordingly with Borchers et al. or Liu et al. [3, 8], three transformation stages, R1, R2, and R3, have been identified. This principal character of the decomposition is independent of the heating rate, as is seen in Fig. 3. Moreover, looking at the details, we were able to distinguish two sub-peaks, R11 and R12, in each DSC curve. The temperatures of the maxima, T_{p11}, and T_{p12}, of these two minor thermal effects being shallow and weak, clearly follow straight lines in the Kissinger heating rate dependence [9] (Fig. 4). We used Kissinger and Elder methods [9, 10] to calculate the activation energies, E^*, and pre-exponential factors, A, for R11, R12, and R2 transformation stages. They are summarized in Table 1.

DSC curves in Fig. 5 show that, after the pre-heating at appropriate temperature, T_a, the multistage dehydrogenation is gradually reacted out, the complex endothermic effect starts at $T_x > T_a$ consuming less heat (and giving less

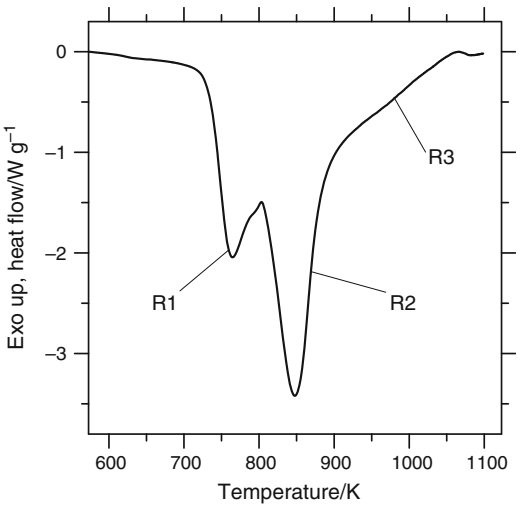

Fig. 2 Subtracted (first minus second run) DSC linear-heating curve from as-produced TiH_2 powder taken at 10 K min^{-1} in argon. Dehydrogenation stages (endothermic peaks) R1, R2, and R3 are identified

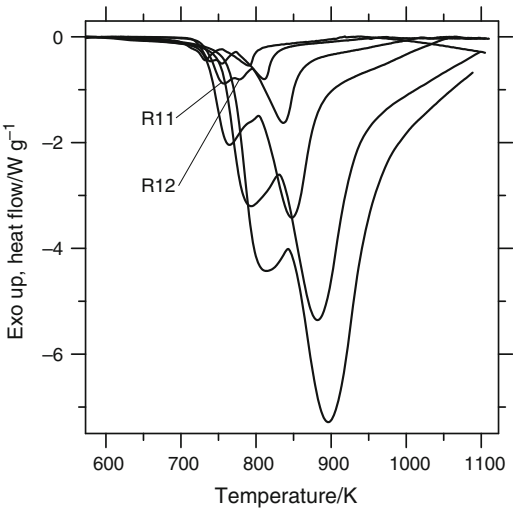

Fig. 3 Heating rate dependence of the DSC curve for as-produced TiH_2 powder. Measurements were done in argon. Heating rates are 1, 2, 5, 10, 20, and 30 K min^{-1}

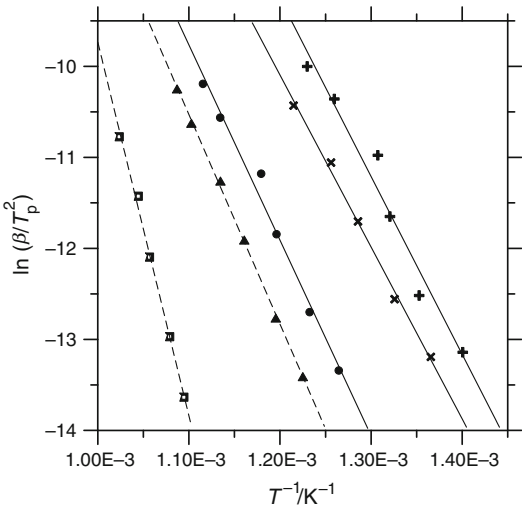

Fig. 4 Linear Kissinger-Elder plots for determination of activation energies and frequency factors of dehydrogenation stages R11 (*plus*), R22 (*times*), R2 (*filled circle*) in as-produced and $R2_{(788,15)}$ (*filled triangle*) in pre-treated at 788 K for 15 min in air TiH_2 powder. Also the apparently linear dependence for oxidation reaction O2 (*open square*) is shown. DTA measurements were done in argon

hydrogen as well [4]). The more extensive is the sample thermal pre-treatment, the less is the remaining total reaction gain in the following measurement. Moreover, in contrast to any pre-treatment in argon [1, 8], the annealing in air, anticipating the presence of oxidation, slightly shifts the following complex endothermic effect to higher temperatures. That shift suggests certain retardation in the dehydrogenation kinetics. The shape of DSC curves (measured in argon) of pre-treated samples does not depend on the heating rate. The Kissinger heating rate dependence of the peak temperature of the $R2_{(788,15)}$ transformation stage (being the R2 stage of the sample isothermally pre-treated in air at 788 K for 15 min) is in Fig. 4, too, and the deduced $E^*_{2,(788,15)}$ and $A_{2,(788,15)}$ are in Table 1.

All calculated activation energies being 157–192 kJ mol^{-1} can be compared with values reported earlier [3, 8, 11]. The obtained evolution of the activation energy with temperature coincides with the values found in [8] or [11] but it contradicts to the dependence deduced by isoconversional methods in [3]. However, as mentioned above, our results gave evidence that the R1 stage consists of two individual sub-stages the extents of which depend on the heating rate (see Fig. 3), and the independence of R1, R2, and eventual higher temperature stages has not been disproved yet. Therefore, we suppose that the variation of an apparent activation energy with temperature, i.e., with the total extent of conversion, α, estimated by any isoconversional method might be only virtual in this specific case. Moreover, our results and all other previous results yielded increased E^* ($\sim$7% in this article) in the case of the presence of oxides in the TiH_2 sample. Thus, the relevant variability in absolute values of E^*, presented in the referred article, might be interpreted also by this reason.

Table 1 Activation energies and pre-exponential factors for dehydrogenation of as-produced (R11, R12, R2), pre-treated at 788 K for 15 min ($R2_{(788,15)}$) and for oxidation (O2) of TiH_2 powder

Reaction stage	E^*/kJ mol^{-1}	A/s^{-1}
R11	162 ± 15	5.0×10^8
R12	157 ± 6	9.5×10^7
R2	179 ± 11	3.9×10^8
$R2_{(788,15)}$	192 ± 3	1.1×10^9
O2	341 ± 13	2.9×10^{16}

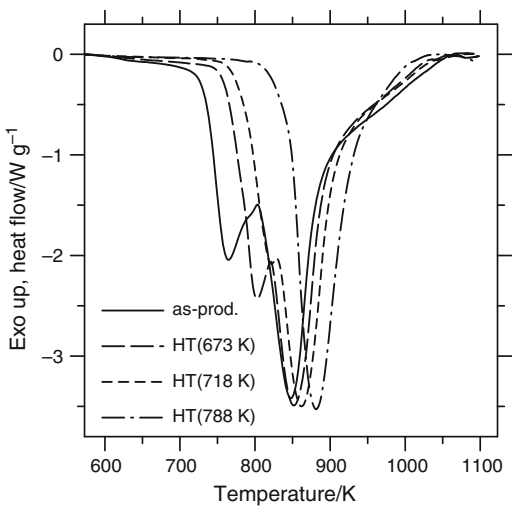

Fig. 5 DSC linear-heating curves of TiH_2 powder pre-treated in air for 15 min taken at 10 K min^{-1} in argon. Annealing temperature is the parameter. Curve for untreated powder is also shown

XRD spectra of our as-produced and pre-treated samples (see Fig. 6) evidenced the presence of oxides, namely Ti_6O and TiO_2 (rutile), in the TiH_2 powder. Weak oxygen traces are already in the non-treated samples. The original Ti-hydride containing 1.924H/Ti has been identified as tetragonal ε-phase. Increasing the temperature, the TiH_2 starts to decompose, H_2 continuously leaves the rigid titanium lattice and both lattice parameters, a and c, continuously change (Fig. 7). Finally, for example, after annealing at 788 K for 15 min, the cubic δ-$TiH_{1.5}$ is detected ($a = 0.4413$ nm). Simultaneously in the presence of an oxygen containing atmosphere, oxygen probably transforms the original lattice with abundance of vacant sites due to released hydrogen and thus increases the content of Ti oxides. At elevated temperatures, due to the advanced escape of H_2, the β-Ti(H) should be formed [3, 8]. At the end of our DTA experiments, the dehydrogenation has been finished and the stable α-Ti is obtained.

SEM images in Fig. 8a and b show that the pre-treatment in air significantly influenced neither the TiH_2 particle size nor the morphology of the particle surface. However, EDX analysis evidenced the presence of oxygen in pre-treated powder. The TEM analysis detected the oxygen being just in the columnar oxide layer systematically growing into each particle from its surface, Fig. 8c.

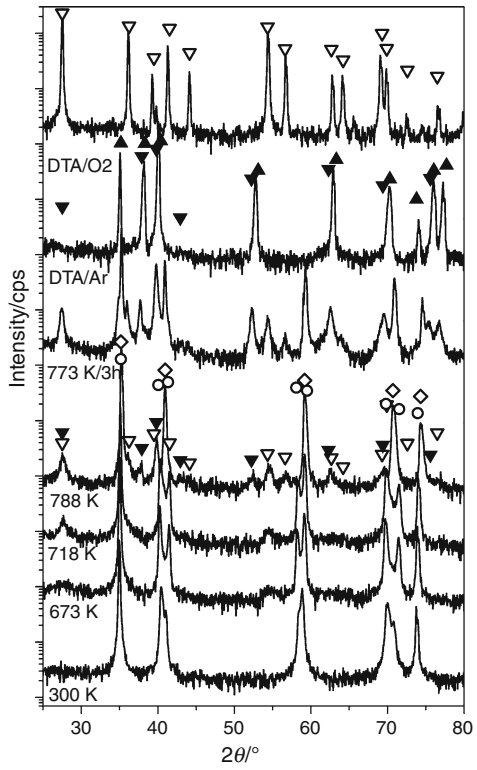

Fig. 6 XRD diffraction patterns of as-produced and heat-treated TiH_2 powder. Heat-treatment is the parameter. *Open circle* ε-$TiH_{1.924}$, *open diamond* δ-$TiH_{1.5}$, *filled triangle* α-Ti, *filled inverted triangle* Ti_6O, *open triangle* TiO_2

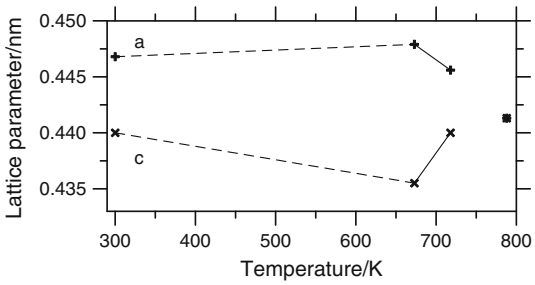

Fig. 7 Dependence of lattice parameters of tetragonal ε-$TiH_{1.924\rightarrow1.5}$ powder on temperature of isothermal annealing. Annealing time was 15 min. *Dashed lines* reflect the effect of lattice dilatation, *solid lines* represent the dehydrogenation of ε-phase, the *points* at 788 K correspond already to the δ-phase

On the base of our results, we can apply and develop the reaction model for the non-isothermal dehydrogenation of TiH_2 powders introduced in Liu et al. [3] and supported by Fig. 9. Because the reactivity between the oxygen and titanium is high, the Ti lattice tends to "absorb" eventual O_2 molecules from the surroundings throughout each particle surface. Simultaneously at $T > T_x$, the powders decompose releasing H_2. First, in the R11 sub-stage, the ε-TiH_x phase changes its composition $TiH_{1.924\rightarrow1.5}$ being then transformed into δ-$TiH_{1.5}$ phase in the R12 sub-stage. In the R2 stage, the β-Ti(H) is formed which is finally transformed into α-Ti(H) and α-Ti in the R3 stage. Dehydrogenation and oxidation are not competitive but rather consecutive reactions in the case of Ti hydride. It means that oxygen (if present) transforms gradually the tetragonal TiH_2 lattice into the tetragonal TiO_2 (rutile) via formation of pure Ti and Ti_6O; however, simultaneously, the new formed Ti–O surface layer slows down the further escape of H_2. While the R11 transformation might proceed continuously from each particle surface into its center as has been suggested in Liu et al. [3], there is not such reason in the case of the formation of β-Ti(H) or α-Ti(H) grains. Thus, in any moment, the variable local composition, (variable local lattice parameter, physical properties, etc.) as well as variable local extend of conversion should exist.

In any case, the relation between the local mechanisms being diffusion [1], surrounding/particle interface reaction [3] or any nucleation and growth mechanisms and the overall rate-controlling mechanism need not to be elementary. It should be searched and, for example, by the DSC kinetic analysis deduced. We have used the Suriñach curve fitting procedure [7]. In this way, each single DSC curve (continuous heating or isothermal) represented in an appropriate coordinate system should correlate with the same master-curve, which is fitted by the most probable theoretical one. The Suriñach analysis of the simplest DSC

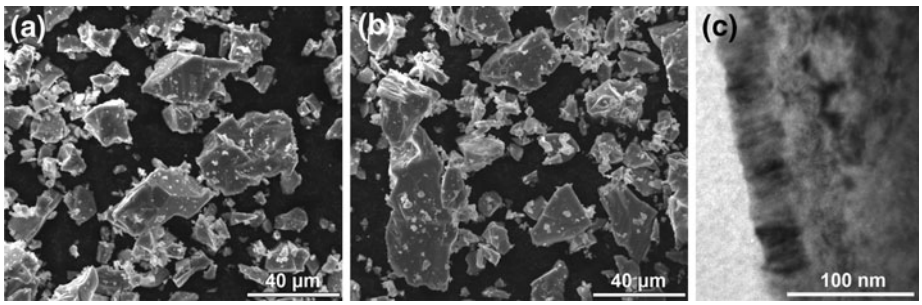

Fig. 8 SEM images of TiH_2 powder ($d < 63$ μm): **a** as-produced; **b** pre-treated in air at 788 K for 15 min. **c** TEM image of the TiH_2 powder particle ($d < 63$ μm) pre-treated in air at 788 K for 15 min. The electron diffraction patterns (not shown) identified TiO_2 in the surface layer and δ-$TiH_{1.5}$ in the core

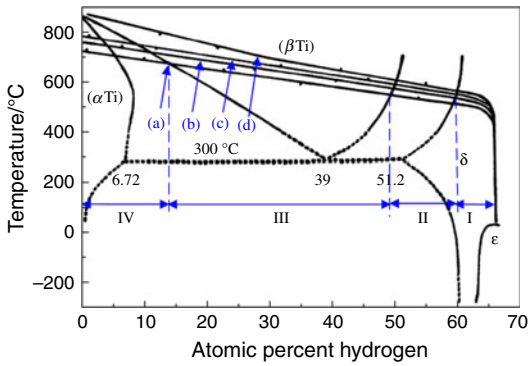

Fig. 9 Ti-H phase diagram combined with the TG curves: **a** 10 K min^{-1}, **b** 15 K min^{-1}, **c** 20 K min^{-1}, **d** 40 K min^{-1} [3]

curve (the dash-and-dotted line in Fig. 5), being the $R2_{(788,15)}$ dehydrogenation stage, is in Fig. 10. It is seen that the Suriñach plots for the six heating rates do not follow one master-curve even in this case. However, they certainly do not represent any diffusion-controlled kinetics (being a convex curve) and they neither represent any interface reaction controlled kinetics (being a straight line). In contrast, they might follow the Johnson–Mehl–Avrami nucleation and growth kinetics [12] with a heating rate dependent exponent $n(\Phi)$. n being initially 3 (three-dimensional interface-controlled growth of already nucleated β-Ti particles or, more probably, decaying homogeneous nucleation and diffusion-controlled three-dimensional growth of the β-Ti phase) should dramatically decrease with proceeding extent of conversion, α. Finally, the JMA kinetics should revert into the normal grain-growth one reaching the exponent $m = 1.5$ (coalescence controlled by the solution of the second phase matrix [13], i.e., coalescence of β-Ti grains in the continuously degrading δ-$TiH_{1.5}$ surroundings). Such result might be accepted taking into account the compositional inhomogeneity in each particle as well as the presence of the R3 stage at higher temperatures.

Oxidation

The typical DSC curve from the linear-heating measurement of TiH_2 powder in oxygen is the full-line in Fig. 11. The XRD spectrum (Fig. 6) of the powder after such DTA

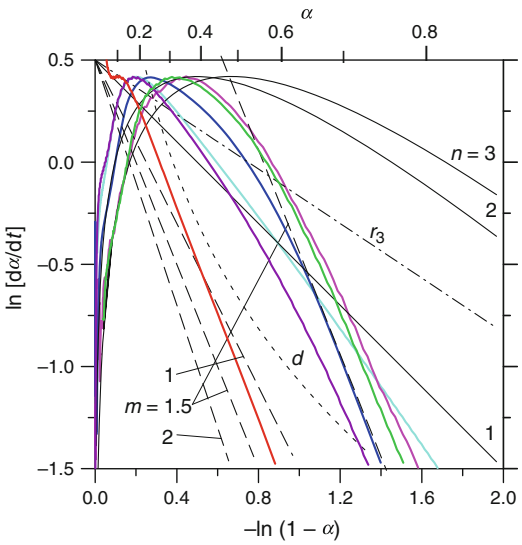

Fig. 10 Suriñach representation of linear-heating dehydrogenation effect $R2_{(788,15)}$ in TiH_2 powder pre-heated in air at 788 K for 15 min. *Colored curves* DTA measurements in argon at 1 K min^{-1} (*solid pink line*), 2 K min^{-1} (*solid green line*), 5 K min^{-1} (*solid blue line*), 10 K min^{-1} (*solid red line*), 20 K min^{-1} (*solid violet line*), and 30 K min^{-1} (*solid turquoise line*). *Black lines* are the theoretical curves for various rate-controlling kinetic laws: JMA nucleation-and-growth (*solid line*) where n is the parameter, interface reaction r_3 (*dash-and-dotted line*), diffusion d (*small dashed line*) and normal-grain-growth (*big dashed line*) where m is the parameter. The lines are vertically shifted to match with the experimental curves. (Color figure online)

measurement shows only the TiO_2 lines. This has attested that both oxidation and dehydrogenation had to take place. Accepting the additivity of thermodynamic quantities and knowing the kinetics of the dehydrogenation (dash-line in Fig. 11), the DSC curves obtained in oxygen and argon atmospheres could be subtracted and the kinetic evolution of the oxidation extracted; it is the dash-and-dotted line in Fig. 11. Thus, the oxidation forms the complicated and large exothermic peak ($\Delta H \sim -13999$ J g^{-1} at $\Phi = 10$ K min^{-1}). It has been divided into two oxidation effects, O1 and O2. The major reaction, O1, is slow; it follows the dehydrogenation kinetics, where both R1 and R2 stages are visible. Probably, it reflects the continuous consecutive replacement of escaping hydrogen by oxygen through a sequence of Ti oxides, finally forming rutile. The reaction O2 is sharp having the explosive character. Both reactions

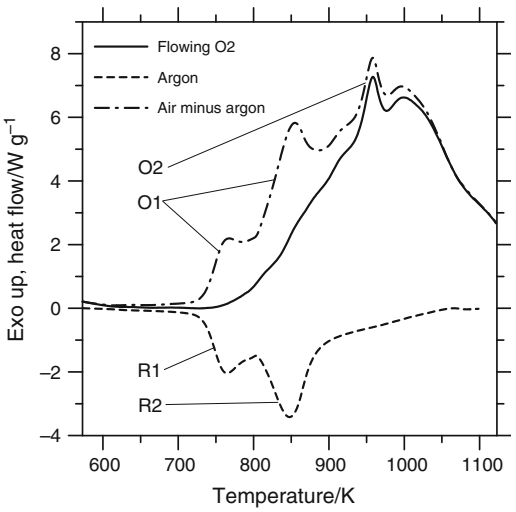

Fig. 11 Subtracted (1 run minus 2 run) DSC linear-heating curve from as-produced TiH_2 powder taken at 10 K min^{-1} in flowing oxygen (*solid line*). Also the measurement in argon (*small dashed line*) and the subtraction of data taken in O_2 and Ar (*dash-and-dotted line*) are shown. Oxidation reactions (exothermic peaks), O1 and O2, are identified

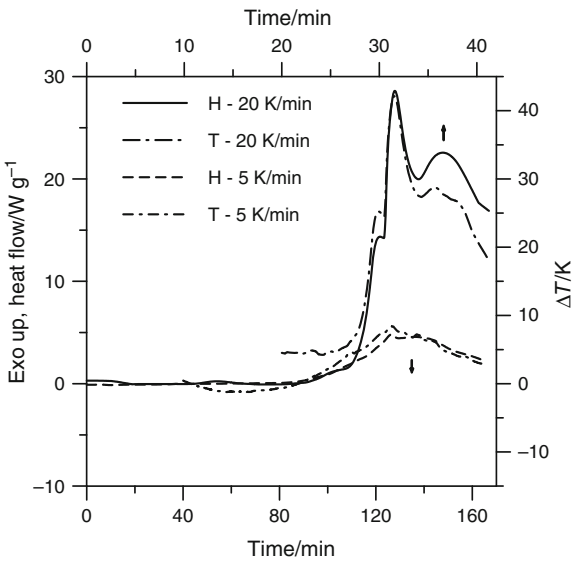

Fig. 12 Proportion between the heat effects, calculated by the DSC mode from the DTA data (H, *full-and-dashed lines*) and over-heatings (T, *dash-and-dotted lines*) of O1 and O2 reactions in as-produced TiH_2 powder taken in DTA in flowing oxygen. Heating rate is the parameter. *Arrows* indicate the corresponding time axes

O1 and O2 have been observed at each heating rate. However, the individual heats, ΔH_{O1}, ΔH_{O2}, are not constant (see Table 2). In any case, the evolved oxidation heat is huge and in the course of DTA experiment it gives rise to considerable overheating of the sample, ΔT, with relation to its surroundings. The absolute value of $\Delta T(T)$ dependence is shown in Fig. 12. Moreover, due to the reaction kinetics ΔT realized in the DTA instrument increases with increasing Φ. Thus, for example, $\Delta T = 40$ K in the case of $\Phi = 20$ K min^{-1} (and ~ 380 K if $\Phi = 30$ K min^{-1}). However, the higher temperature gradient between the sample and the surrounding invokes the higher thermal losses across the interface. This variability in the non-trivial thermal losses toward the sample's surrounding might be responsible for the variability in the measured reaction heats as, for example, in the case of ΔH_{O1} (see Table 2). Therefore, the DTA should record apparent oxidation effects, which consist of the true, constant reaction heat and the variable thermal losses (in fact a difference between the thermal losses of the sample and the reference) increasing proportionally to ΔT. Then, the true ΔH_{O1} might be obtained extrapolating its dependence on ΔT to zero.

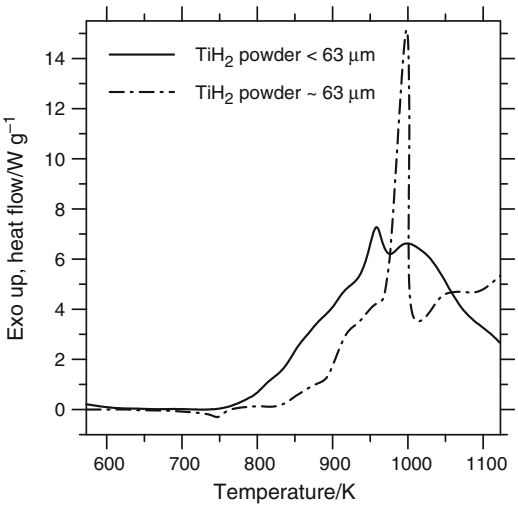

Fig. 13 Variability of the oxidation kinetics with the quality of the as-produced TiH_2 powder. Diameter of the grains is the parameter. Taken in DTA at 10 K min^{-1} in flowing oxygen

Table 2 Heats of O1 and O2 oxidation reactions, and the overheating produced in TiH_2 powder as dependences of heating rate

Φ/K min^{-1}	ΔH_{O1}/J g^{-1}	ΔH_{O2}/J g^{-1}	ΔT_{O2}/K
1	−9017	−997	0.9
2	−10551	−391	1.0
5	−13038	−67	0.7
10	−13707	−294	3.7
20	−14282	−1334	14.5
30			381.1

The reaction O2 seems to be more complicated. The proportionality between ΔH_{O2} and Φ is not simple (see Table 2). Moreover, the onset temperature, $T_{x,O2}$, and heat effect of O2 depend on the quality of the TiH_2 powder as it can be seen in Fig. 13 and on the purity of the atmosphere too. In any case, increasing $T_{x,O2}$ increases also the ΔH_{O2} at the expense of ΔH_{O1}. Due to this fact, the kinetic

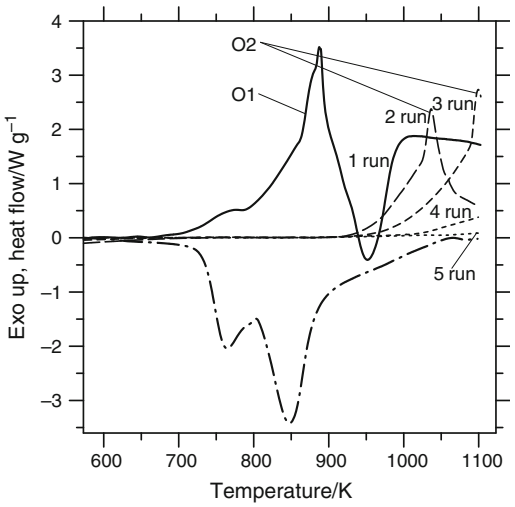

Fig. 14 Sequence of 6 subtracted (current minus 6th run) DSC linear-heating curves from as-produced TiH_2 powder taken at 10 K min^{-1} in static air. Oxidation reactions (exothermic peaks) O1 and O2 are identified. Also the measurement in argon (*dash-and-dotted line*) is shown

parameters of O2 determined by Kissinger–Elder methods (Fig. 4) and presented in Table 1 might be false. We suppose that the appearance of this explosive reaction might be related to the dimensions of the powder grains, i.e., to their diameter, surface, or volume. The O2 reaction is independent of the pre-treatment and it proceeds in dehydrogenated samples too (in this case above 1042 K). It means that it is either independent of the presence of hydrogen, it appears when α-Ti starts to be formed, or it is initialized when the escape of H_2 is finished.

TiH_2 degradation in static air

As shown above, the decomposition of TiH_2 powder proceeds independently of the atmosphere. Contrariwise, the oxidation is dependent on the access of oxygen. The more hindered is the oxygen inlet, the slower and more peculiarly the oxidation manifests itself. Thus, for example, in the case of linear heating in static air when the sample lies deeply in a profound container (sample pan), the oxidation starts regularly and then stops above 900 K when all oxygen, located in the container, has been reacted and the stream of liberated hydrogen prevents further inlet of additional oxygen (the full-line up to 950 K in Fig. 14). Later, when the dehydrogenation is completed (represented by the endothermic dash-and-dotted line in Fig. 14), a new O_2 molecule might reach the sample and the oxidation might continue at higher temperatures again (the full-line above 950 K in Fig. 14). But in any case, the O2 reaction does not start and the rate of the O1 reaction is limited by the partial diffusivity of O_2 molecules in the ambient air. Therefore, the typical plateau in the DSC curve is formed [14]. The O2 reaction can start in the next heating run and both reactions only slowly decay in the sequence of several subsequent heating runs.

Conclusions

In the oxygen containing atmosphere, two consecutive reactions, namely the dehydrogenation and the oxidation, take part in TiH_2 powder at approximately same elevated temperatures.

- Dehydrogenation is initialized by temperature. It advances continuously, from the surface of each particle to its center, having three distinct stages (R1, R2, and R3). The major decomposition stage, R2, is controlled by the JMA nucleation-and-growth and modified coalescence reaction kinetics. The dehydrogenation might be slightly decelerated by eventual oxidation.
- Appropriate thermal treatment shifts the dehydrogenation to higher temperatures; however, it lowers the gain of hydrogen.
- Oxidation takes place consecutively, having two types (O1 and O2). O1 reaction is slow; it is controlled by the kinetics of the dehydrogenation. O2 reaction is explosive; its initialization temperature depends on the morphology of the TiH_2 powder. The overall oxidation produces giant heat causing risky overheating.
- Oxidation slightly shifts the dehydrogenation to higher temperatures. Limiting the supply of oxygen does not influence the dehydrogenation; however, it might control the oxidation and its heat production.

Acknowledgements Support of the Agency of the Ministry of Education of the Slovak Republic for the Structural Funds of the EU (CEKOMAT I, ITMS 26240120006) is gratefully acknowledged. The research was supported also by the projects VEGA 2/0157/08, APVV-0102–07, APVV-0736-07 "LOWCOSTFOAM" and by the CEX SAS "NANOSMART."

Appendix

(i) The Kissinger–Elder relation [9, 10] is

$$\ln\left[\Phi/T_p^2\right] = \ln[(AR)/E^*] + \ln f_m(\max) - E^*/(RT_p),$$

where A and E^* are parameters being pre-exponential factor and activation energy, Φ is the heating rate, T_p is the DSC peak temperature, R is the gas constant and $\ln f_m(\max) = -0.485$.

(ii) The Suriñach representation [7] is

$$\ln[\mathrm{d}\alpha(T,t)/dT] + [E^*/RT(t)] + \ln\ \Phi \text{ versus } -\ln\,[1-\alpha(T,t)]$$

or

$$\ln[\mathrm{d}\alpha(t)/\mathrm{d}t]_{\mathrm{Ta}} + E^*/[RT_{\mathrm{a}}] \text{ versus } -\ln\,[1-\alpha_{\mathrm{Ta}}(t)]$$

where T is temperature, t is time, $\alpha(T, t)$ is the extent of conversion, $\mathrm{d}\alpha(T, t)/\mathrm{d}T = y(T, t)$ or $[\mathrm{d}\alpha(t)/\mathrm{d}t]_{\mathrm{Ta}} = y(t)_{\mathrm{Ta}}$ is the continuous heating or isothermal signal in a power-compensation DSC. E^* already has to be known.

(iii) The simplified fundamental differential equation for a quantitative DTA [15] is

$$\begin{aligned}\Delta H\mathrm{d}\alpha(t)/\mathrm{d}t + C_{\mathrm{p}}\mathrm{d}T/\mathrm{d}t = {} & \Delta T_{\mathrm{S-R}}(t)/K(t) \\ & + \Delta T_{\mathrm{S-E}}(t)/K(t) \\ & - \Delta T_{\mathrm{R-E}}(t)/K(t) \\ & + [\tau/K(t)]\mathrm{d}[\Delta T(t)]/\mathrm{d}t,\end{aligned}$$

where ΔH is the heat generated or absorbed by the sample, C_{p} is the heat capacity of the sample, $K(t)$ is the thermal exchange coefficient being the calibration function of the measuring system, $\Delta T_{\mathrm{S-R}}$, $\Delta T_{\mathrm{S-E}}$ and $\Delta T_{\mathrm{R-E}}$ are the temperature gradients between the sample (S), reference (R) and environment (E), τ is the time constant of the system. In the case of a sharp and massive reaction, the contribution of C_{p} term, the heat losses between the reference and its surrounding as well as the differential term might be neglected with relation to the huge contributions of the terms proportional to $\Delta T_{\mathrm{S-R}}$ and $\Delta T_{\mathrm{S-E}}$. Thus the area of the DSC peak represents not only the heat of the reaction but also the heat losses between the sample and its surrounding, namely

$$\int \Delta T_{\mathrm{S-R}}(t)/K(t)\mathrm{d}t = \Delta H - \int \Delta T_{\mathrm{S-E}}(t)/K(t)\mathrm{d}t.$$

References

1. Matijasevic-Lux B, Banhart J, Fiechter S, Görke O, Wanderka N. Modification of titanium hydride for improved aluminium foam manufacture. Acta Mater. 2006;54:1887–900.
2. Nosko M, Simančík F, Florek R. Reproducibility of aluminum foam properties: effect of precursor distribution on the structural anisotropy and the collapse stress and its dispersion. Mater Sci Eng. 2010;A527:5900–8.
3. Liu H, He P, Feng JC, Cao J. Kinetic study on nonisothermal dehydrogenation of TiH_2 powders. Int J Hydrog Energy. 2009; 34:3018–25.
4. Fenández JF, Cuevas F, Sánchez C. Simultaneous differential scanning calorimetry and thermal desorption spectroscopy measurements for the study of the decomposition of metal hydrides. J Alloy Compd. 2000;298:244–53.
5. Kennedy AR, Lopez VH. The decomposition behavior of as-received and oxidized TiH_2 foaming-agent powder. Mater Sci Eng. 2003;A357:258–63.
6. Bhosle V, Baburaj EG, Miranova M, Salama K. Dehydrogenation of TiH_2. Mater Sci Eng. 2003;A356:190–9.
7. Suriñach S, Baró MD, Calvaguera-Mora MT, Clavaguera N. Kinetic study of isothermal and continuous heating crystallization in $GeSe_2$-GeTe-Sb_2Te_3 alloy glasses. J Non-Cryst Solids. 1983; 58:209–17.
8. Borchers Ch, Khomenko TI, Leonov AV, Morozova OS. Interrupted thermal desorption of TiH_2. Thermochim Acta. 2009; 493:80–4.
9. Kissinger HE. Reaction kinetics in differential thermal analysis. Anal Chem. 1957;29:1702–6.
10. Elder JP. The general applicability of the Kissinger equation in thermal analysis. J Therm Anal. 1985;30:657–69.
11. Yang HD, Hur Y, He P, Yang SR. Effect of decomposition properties of titanium hydride on the foaming process and pore structures of Al alloy melt foam. Mater Sci Eng. 2007; A445–446:415–26.
12. Christian JW. The theory of transformations in metals and alloys. New York: Pergamon Press; 1965.
13. Atkinson HV. Theories of normal grain growth in pure single phase systems. Acta Metall. 1988;36:469–91.
14. Illeková E, Czomorová K. Kinetics of oxidation in various forms of carbon. J Therm Anal Calorim. 2005;80:103–8.
15. Illeková E, Aba B, Kuhnast FA. Measurements of accurate specific heats of metallic glasses by differential scanning calorimetry (DSC). Part 1. Analysis of theoretical principles and accuracies of suggested measurement procedures. Thermochim Acta. 1992; 195:195–209.